NASA Contractor Report 178111

ICASE REPORT NO. 86-39

ICASE

INCIPIENT TRANSITION PHENOMENA IN COMPRESSIBLE FLOWS OVER A FLAT PLATE

Gordon Erlebacher
M. Yousuff Hussaini

Contract Nos. NAS1-17070, NAS1-18107
June 1986

INSTITUTE FOR COMPUTER APPLICATIONS IN SCIENCE AND ENGINEERING
NASA Langley Research Center, Hampton, Virginia 23665

Operated by the Universities Space Research Association

National Aeronautics and
Space Administration

Langley Research Center
Hampton, Virginia 23665

Incipient Transition Phenomena in Compressible Flows over a Flat Plate

G. Erlebacher
NASA Langley Research Center. Hampton, VA

M.Y. Hussaini
Institute for Computer Applications in Science and Engineering

ABSTRACT

The full three-dimensional time-dependent compressible Navier-Stokes equations are solved by a Fourier-Chebyshev method to study the stability of compressible flows over a flat plate. After the code is validated in the linear regime, it is applied to study the existence of the secondary instability mechanism in the supersonic regime.

The second author's research was supported under the National Aeronautics and Space Administration under NASA Contract No. NAS1-17070 and NAS1-18107 while he was in residence at the Institute for Computer Applications in Science and Engineering (ICASE), NASA Langley Research Center, Hampton, VA 23665-5225.

1. Introduction

Although the predominant interest in the stability and transition to turbulence lies in compressible flows, research undertaken over the past 15 years has mainly focused on incompressible phenomena because of their comparative simplicity. As a result, a fairly extensive collection of theoretical [1,2], experimental [3,4] and numerical [5,6] data has been accumulated and cross-correlated for incompressible channel and Blasius boundary-layer flows. Detailed studies of several instability mechanisms has led to a fairly comprehensive picture of the incipient stages of transition in incompressible flows. One such mechanism involves the interaction of a two-dimensional primary unstable wave with two skewed waves. This secondary instability leads to what is commonly referred to as K-type breakdown whose signature is a peak-valley vortical structure [1]. These structures have been successfully simulated numerically for incompressible boundary-layer flows [5,6]. Moreover, results from these simulations agree very well with theoretical and experimental findings.

As a step towards a better understanding of the instability mechanisms in compressible flows, the K-type breakdown of laminar flow at high Mach numbers is studied in this report. To this end, a three-dimensional, fully-spectral compressible Navier-Stokes code capable of direct simulation of parallel boundary-layer flows over a flat plate has been developed. The code is first validated in the linear regime against the unstable eigenfunctions of the compressible linear stability eigenvalue problem. Then the temporal evolution of a triad of waves superimposed on a parallel boundary-layer is followed up to the incipient breakdown.

2. Equations

The full unsteady, three-dimensional, compressible Navier-Stokes equations expressed in non-dimensional form are

$$\frac{\partial \rho}{\partial t} + \nabla\cdot(\rho\vec{v}) = 0, \tag{1}$$

$$\frac{\partial \rho\vec{v}}{\partial t} + \nabla\cdot(\rho\vec{v}\vec{v}) = -\nabla p + \frac{1}{R_e}\nabla\cdot\vec{\tau} + \vec{F}_{\rho\vec{v}}, \tag{2}$$

$$\frac{\partial p}{\partial t} + \vec{v}\cdot\nabla p = -\gamma p\nabla\cdot\vec{v} + \frac{1}{P_r R_e M_\infty^2}\nabla\cdot(\mu\nabla T) + \Phi + F_p \tag{3}$$

and

$$\gamma M_\infty^2 p = \rho RT \tag{4}$$

where $\vec{v}$ is the velocity vector (u,v,w), ρ the density, T the temperature, p the pressure, $\vec{\tau}$ the viscous stress-tensor

$$\vec{\tau} = \mu\,(\nabla\vec{v} + \nabla\vec{v}^{\,T}) + \lambda\nabla\cdot\vec{v}\,\vec{I}, \tag{5}$$

and Φ is the dissipation function

$$\Phi = \frac{\mu}{2}\,(\nabla\vec{v} + \nabla\vec{v}^{\,T})^2 + \lambda(\nabla\cdot\vec{v})^2. \tag{6}$$

The first and second viscosity coefficients μ and λ are related by the assumption of zero bulk viscosity

$$\lambda + \frac{2}{3}\mu = 0. \tag{7}$$

$\vec{F}_{\rho\vec{v}} = (F_{\rho u}, F_{\rho v}, 0)$ and F_p are source terms that are described later. Variables have been non-dimensionalized as follows: distance with respect to boundary-layer displacement thickness δ^*, velocity, temperature and density with respect to their free-stream values $\bar{U}_\infty$, $\bar{T}_\infty$, $\bar{\rho}_\infty$ and pressure with respect to the dynamic pressure $\bar{\rho}_\infty \bar{U}_\infty{}^2$. Viscosity and conductivity are scaled with respect to their free-stream values $\bar{\mu}_\infty$ and $\bar{\kappa}_\infty$. With these definitions, the Reynolds number becomes

$$R_e = \frac{\bar{\rho}_\infty\,\delta^*\,\bar{U}_\infty}{\bar{\mu}_\infty}. \tag{8}$$

In this report the Prandtl number

$$P_r = \frac{C_p\,\bar{\mu}}{\bar{\kappa}} \tag{9}$$

is assumed constant and equal to 0.72. C_p is the specific heat at constant pressure. We assume a temperature dependent viscosity given by the non-dimensional form of Sutherland's law

$$\mu(T) = \frac{(1 + \frac{196.8}{T_\infty})}{(T + \frac{196.8}{T_\infty})}\,T^{\frac{3}{2}}. \tag{10}$$

In incompressible boundary-layer flows, it has been observed that the evolution to transition of ribbon-excited Tollmien-Schlichting (TS) waves occupies a space of approximately ten wavelengths [3]. An adequate resolution of the boundary-layer in all three directions over a ten wavelength streamwise distance would exceed

the present capability of today's most powerful computers. In incompressible simulations this difficulty has been circumvented by the assumption of spatial periodicity in the two directions parallel to the plate [5], allowing the set up of a properly posed initial-value problem. This assumption allows the computational domain to be restricted to one TS wavelength in both the streamwise and spanwise directions. A similar periodicity assumption is made in the present work to make the compresssible simulations computationally tractable. In order that the mean parallel boundary-layer flow be a stationary solution to the Navier-Stokes equations, source terms must be added to equations (1)-(3). The forcing terms are given by

$$F_{\rho u} = \frac{1}{R_e}\frac{\partial}{\partial z}(\mu\frac{\partial U_m}{\partial z}) \tag{11}$$

$$F_{\rho v} = \frac{1}{R_e}\frac{\partial}{\partial z}(\mu\frac{\partial V_m}{\partial z}) \tag{12}$$

$$F_p = \frac{1}{R_e P_r M_\infty^2}\frac{\partial}{\partial z}(\mu\frac{\partial T_m}{\partial z}) + \frac{1}{R_e}[(\frac{\partial U_m^2}{\partial z})^2 + (\frac{\partial V_m^2}{\partial z})^2] \tag{13}$$

In obtaining these relations mean pressure is taken constant across the boundary-layer, the mean velocity has non-zero streamwise ($U_m(z)$) and spanwise ($V_m(z)$) components, and the mean temperature is $T_m(z)$. In what follows, V_m is set to zero.

3. Algorithm

The system of equations (1-4) is solved in conservative form under the parallel flow assumption. Periodicity boundary-conditions in the streamwise and spanwise directions permit a Fourier representation of the primitive variables u, v, w, p and ρ. For example, the double Fourier decomposition of u is

$$u(x,y,z,t) = \sum_{m=-\frac{N_x}{2}}^{\frac{N_x}{2}-1}\sum_{n=-\frac{N_y}{2}}^{\frac{N_y}{2}-1} u_{i,j}(z,t)\, e^{i\,(m\alpha x+n\beta y)} \tag{14}$$

where N_x and N_y are the total number of nodes in x and y directions. The periods of the physical domain in the streamwise and spanwise directions (L_x and L_y) are related to the wave numbers α and β by $L_x=\frac{2\pi}{\alpha}$ and $L_y=\frac{2\pi}{\beta}$. The code has the option to evaluate normal spatial derivatives either by finite-difference approximation or by a Chebyshev collocation method, in which case $u_{ij}(z,t)$ has the series representation

$$u_{ij}(z,t) = \sum_{k=1}^{N_z} u_{ijk}(t)\, T_k(z)$$

where $T_k(z)$ is the Chebyshev polynomial of order k. The number of nodes in the normal direction is N_z. In the absence of discontinuities in the solution, spectral collocation methods are far more accurate than typical finite-difference methods for a specified distribution of a fixed number of nodes. The physical domain (0, z_{max}) in the direction normal to the plate is mapped onto the computational domain with an algebraic mapping which takes the form

$$z = \frac{z_{1/2}\, z_{max}\, (1+\eta)}{z_{max} - \eta\, (z_{max} - 2\, z_{1/2})}$$

for the spectral representation in the normal direction and

$$z = \frac{z_{max}\, z_{1/2}\, \xi}{(z_{max} - z_{1/2}) + \xi\, (2z_{1/2} - z_{max})}$$

when finite-differences are used. In the latter case, the computational variables ξ ranges from 0 to 1. In terms of ξ, the standard Chebyshev spectral node distribution is given by

$$\eta = -\cos(\pi\xi)\ ,$$

One half the normal nodes are located between z=0 and z=$z_{1/2}$.

In all the mean flow calculations considered thus far, the critical layer is always found to lie between δ^* and $1.5\delta^*$ from the wall and special care is excercised to resolve it. Setting $z_{1/2}$=2 is found to be optimal for resolving the relevant flow structure in the chosen parameter range.

Currently, the code is fully explicit. A third order low-storage Runge-Kutta method [8] is used for time discretization. For the equation

$$U_t = F,$$

such a scheme leads to

$$H_1 = F_0$$

$$U_1 = U_0 + \frac{1}{3} H_1$$

$$H_2 = \delta t\, F_1 - \frac{5}{9} H_1$$

$$U_2 = U_1 + \frac{15}{16} H_2$$

$$H_3 = \delta t\, F_2 - \frac{153}{128} H_2$$

$$U_3 = U_2 + \frac{8}{15} H_3$$

which only requires two storage arrays per variable. Theoretically the scheme is unconditionally stable for a CFL below 0.55; however it is empirically found that above a CFL of 0.2 that the algorithm is unstable. The time step is thus limited by

$$\Delta t < 0.2 \min_{grid} [\frac{\Delta x}{u} + \frac{\Delta y}{v} + \pi \frac{\Delta z}{w}] .$$

4. Initial Conditions

The initial conditions consist of a triad of waves superimposed on a mean flow. Mean flow profiles are generated from the solution to the similar compressible boundary-layer equations with zero pressure gradient and zero heat transfer at the wall. In non-dimensional form, these are [9]

$$f f'' + (\mu \rho f'')' = 0 ,$$

$$\frac{1}{P_r} (\mu \rho T')' + f T' + (\gamma-1) M_\infty^2 \mu \rho T_1 f''^2 = 0 ,$$

$$\rho T = 1 ,$$

with boundary conditions

$$f(0) = f'(0) = 0 ,$$

$$f'(\infty) = 1 ,$$

$$T(\infty) = 1 ,$$

$$T'(0) = 0 .$$

A prime denotes differentiation with respect to the similarity variable

$$\eta = c(M_\infty, T_\infty) \frac{\overline{Z}}{\sqrt{2}} \frac{U_\infty \delta^*(x) \rho_\infty}{\mu_\infty} = \frac{\overline{Z}}{\sqrt{2}} R_\epsilon(x) \qquad (15)$$

where $\bar{Z}$ is related to the normal coordinate z by the transformation

$$\bar{Z} = \int_0^z \rho \, dz$$

The coefficient c in (15) is a function of free-stream temperature and Mach number.

The stability of flows is studied at a prescribed supercritical Reynolds number $R_e(x_0)$. After freezing the streamwise dependence of the mean flow profiles at $x=x_0$, they are extended over the entire plate. Thus, the displacement thickness is constant, and the mean flow is a function only of the coordinate normal to the plate. The normal velocity component is set to zero, and $U_m = f'(\eta)$.

In the simulation which is to be described, the mean flow is initially perturbed by a 2-D Tollmien-Schlichting wave and two 3-D waves. For example, when perturbed by a single wave, the initial streamwise velocity is the real part of

$$u = U_m + \tilde{u}(z) \, e^{i(\alpha x + \beta y - \omega t)}$$

for real streamwise and spanwise wavenumbers α and β. Similar relations hold for the remaining variables. The complex growth rate ω is calculated by an eigenvalue code [10]. From the real part of ω, the period of the wave can be determined. Growth or decay of the wave depends on the sign of ω_i , the imaginary part of ω. A stable wave corresponds to ω_i negative, while a positive ω_i indicates a growing mode.

5. Boundary conditions

Under the assumption of parallel flow, all the variables are periodic in the streamwise and spanwise directions. No slip conditions are applied to the velocities at the wall which is adiabatic. In the far-field, all the variables are frozen at their initial values.

6. Results

The coordinate system and nomenclature used for the flat plate geometry is illustrated in figure 1. Complex eigenfunctions and eigenvectors are obtained by numerically solving the eigenvalue problem associated with the linear stability of compressible parallel flows [10]. Table I summarizes the input parameters. Mean streamwise velocity and mean temperature profiles at Mach 0.5 and 4.5 are compared with each other in figures

2-3. As seen from figure 2, at Mach 4.5 the mean temperature across the boundary-layer varies by more than a factor of 4. This is in sharp contrast with the flat temperature profiles at Mach 0.5 (fig. 3). The complex eigenfunctions are normalized to insure a maximum streamwise perturbation velocity of unity. Streamwise velocity profiles are illustrated in figures 4-5. With the normalization imposed on the eigenfunctions, it is immediately apparent from figure 6 that the extrema of the temperature variation are much more severe at the higher Mach number.

Added to the mean flow, the computed three-dimensional eigenfunctions serve as initial flow-field data for the full Navier-Stokes code. For example, the initial streamwise velocity distribution is

$$U(z) = U_m + \varepsilon_{2D} \cos(\theta(z)+\alpha x+\beta y)$$

where $\theta(z)$ is the phase of the streamwise velocity eigenfunction. Similar relations are satisfied by the remaining velocity components, pressure and density. A value of .001 for ε_{2D} is sufficient to insure the absence of non-linear interactions of the fundamental mode with its higher harmonics. Figures 7-8 summarize the results of the linear test. Plotted in these figures is $log(E_K)$ versus time, where E_K is the perturbed kinetic energy

$$E_K = \frac{1}{2}\int \rho_m \left[(u-U_m)^2 + v^2 + w^2\right] dx\, dy\, dz\ .$$

Comparisons of the growth rates predicted by the Navier-Stokes code against linear results are made using both Chebyshev collocation and finite-differences in the direction normal to the wall. At Mach 0.5, the growth curves of perturbed kinetic energy for a 33 collocation point normal distribution and a distribution with 129 finite-difference nodes are almost indistinguishable from each other and from the growth predicted by the linear eigenvalue code. However, 65 Chebyshev collocation nodes are required to match the predicted linear growth curves at Mach 4.5. In this case, 129 finite-difference nodes are not sufficient to resolve the structure of the eigenfunctions near the wall. The need for extra resolution at the higher Mach number is explained by the more complicated structure of the eigenfunctions presented in figures 5 and 6b. At Mach 4.5, the displacement thickness is almost an order of magnitude greater than at Mach 0.5, but in units of δ^*, the distance of the critical layer from the wall always lies between 1 and 1.5.

For the non-linear simulation, the parameters are: M_∞=4.5, R_ϵ=10000, $\overline{T}_\infty$=110.85°R, α=.6 and β=1.03923. The spanwise wavenumber is chosen to maximize the growth rate of the 3-D mode in order to accelerate the

onset of the instability. The initial wave angle of the three-dimensional wave is 60° .

The amplitudes of the 2-D and 3-D waves are respectively ε_{2D} and ε_{3D} . Initially, the flow variables are set to

$$u(x,y,z) = U_m + \varepsilon_{2D}(z)\cos(\theta_{u_{2D}}(z) + \alpha x + \beta y) +$$
$$\varepsilon_{3D} u_{3D}\,[\cos(\theta_{u_{3D}}(z) + \alpha x + \beta y) + \cos(\theta_{u_{3D}}(z) + \alpha x - \beta y)]$$

$$v(x,y,z) = \varepsilon_{2D}(z)\, v_{2D}\cos(\theta_{v_{2D}}(z) + \alpha x + \beta y) +$$
$$\varepsilon_{3D}\, v_{3D}\,[\cos(\theta_{v_{3D}}(z) + \alpha x + \beta y) - \cos(\theta_{v_{3D}}(z) + \alpha x - \beta y)]$$

$$w(x,y,z) = \varepsilon_{2D}\, w_{2D}(z)\cos(\theta_{w_{2D}}(z) + \alpha x + \beta y) +$$
$$\varepsilon_{3D}\, w_{3D}\,[\cos(\theta_{w_{3D}}(z) + \alpha x + \beta y) + \cos(\theta_{w_{3D}}(z) + \alpha x - \beta y)]$$

$$\rho(x,y,z) = \rho_m + \varepsilon_{2D}\,\rho_{2D}(z)\cos(\theta_{\rho_{2D}}(z) + \alpha x + \beta y) +$$
$$\varepsilon_{3D}\,\rho_{3D}\,[\cos(\theta_{\rho_{3D}}(z) + \alpha x + \beta y) + \cos(\theta_{\rho_{3D}}(z) + \alpha x - \beta y)]$$

$$p(x,y,z) = p_m + \varepsilon_{2D}\, p_{2D}(z)\cos(\theta_{p_{2D}}(z) + \alpha x + \beta y) +$$
$$\varepsilon_{3D}\, p_{3D}\,[\cos(\theta_{p_{3D}}(z) + \alpha x + \beta y) + \cos(\theta_{p_{3D}}(z) + \alpha x - \beta y)]$$

Starting amplitudes are ε_{2D}=.054 and ε_{3D}=.012. The 2-D growth rate predicted by linear theory is ω_{2D}=.5011+.00203i with a period of T=12.54. The 3-D growth rate, ω_{3D}=.09765+.01098i, is substantially larger than its 2-D counterpart, a property typical of compressible flows as the Mach number increases. Above Mach 3, the phase angle that produces maximum growth is between 55° and 65° [2]. As stated earlier, the primitive variables are expanded in Fourier series in the x and y directions. The (i,j) mode of u is defined by the coefficient $u_{i,j}$ in (14). Figure 9 shows the evolution of the kinetic energy of selected modes as a function of time. The energy content of mode (i,j) is defined by

$$E_{ij} = \log_{10}\left(\int \frac{u_{ij}^2 + v_{ij}^2 + w_{ij}^2}{E_m}\, dz\right).$$

The energy content of the (1,0) mode remains fairly constant. The spanwise modes (0,1) and (0,2) continuously

grow until their strength is apparently sufficient to trigger the growth of the (1,1) mode, which is largely responsible for the presence or absence of the secondary instability. Prior to the rapid growth of the (1,1) mode, it goes through a stable interval starting at about 3 periods. Once the (0,1) mode is within 0.5 decades of the fundamental 2-D mode, the (1,1) mode suddenly becomes unstable again. At this stage, non-linear interactions between the 2-D and the 3-D mode begin to dominate the evolution of the flow.

Spanwise vorticity contours are illustrated in figure 10 in successive spanwise planes (normal to the spanwise direction) in the peak and adjacent planes. The initial formation of the high-shear layer after 5.5 periods (computed on a 36x16x65 grid) is apparent in this figure. The downward curving of the shear layer near its maximum is similar to the structure found in incompressible flow in the early stages of transition [5,6]. Streamwise and spanwise vorticity contours in streamwise planes (the normal to the plane is in the streamwise direction) are shown in figures 11-12 after 5.5 periods in planes at 0.0, 0.25, 0.5 and 0.75 wavelengths along the streamwise direction. Saddle points in the spanwise vorticity correspond to maximum streamwise vorticity. If these maxima are followed in figures 12a-d, the uplifting of the vortex tube becomes apparent, although it is rather flat.

7. Conclusions

A fully spectral, 3-D, compressible Navier-Stokes code specialized to parallel flow over a flat plate has been presented. It has been demonstrated that in the linear regime an initial eigenfunction grows at the same rate as predicted by a linear eigenvalue code in both subsonic and supersonic flow. As a test of the non-linear behaviour of the code at high Mach numbers, initial conditions are set up to numerically generate, for the first time, a high Mach number peak-valley vortical structure similar to that observed and computed for incompressible flows.

8. Acknowledgements

The authors are thankful for the many fruitful discussions with T. Zang. The authors would also like to acknowledge the staff of the Numerical Aerodynamic Simulator at the NASA Ames Research Center for their support in the use of the CRAY 2 during its initial operational period. Without this support this calculation would not have been possible.

9. Table

Case	Mach nb.	α	β	R_e	T_∞ (°R)
I	0.5	.24933	.20944	1200	520.00
II	4.5	.4652	.8057	10000	110.85

Table I: parameters input to the linear eigenvalue code

10. References

[1] Herbert, T.: Secondary Instability of Plane Channel Flow to Subharmonic Three-Dimensional Disturbances. Phys. Fl., Vol. 26, No. 4, 1983, pp. 871-874.

[2] Mack, L.M.: Boundary-Layer Linear Stability Theory. AGARD, Report 709.

[3] Kovasznay, L.S., Komoda, H. and Vasudeva, B.R., Proc. of the 1962 Heat Transfer and Fluid Mech. Inst., pp. 1-26, Stanford University Press, 1962.

[4] Saric, W. S.: Experiments on the Subharmonic Route to Transition. Turbulence and Chaotic Phenomena in Fluids, ed: T. Tatsumi, North-Holland, 1984.

[5] Wray, A. and Hussaini, M.Y.: Numerical experiments in Boundary-layer Stability. Proc. R. Soc. Lond. 392, pp. 373--389, 1984.

[6] Zang, T.A. and Hussaini, M.Y.: Numerical Experiments on Subcritical Transition Mechanisms. AIAA Paper 85-0296, 1985.

[7] Zang, T.A. and Hussaini, M.Y.: Numerical Experiments on the Stability of Controlled Shear Flows. AIAA paper 85-1698, 1985.

[8] Williamson, J.H.: Low Storage Runge-Kutta Schemes. J. Comp. Phys. 35, 48-56, 1980.

[9] Stewartson, K.: The Theory of Laminar Boundary-Layers in Compressible Fluids. Oxford Mathematical Monographs, 1964.

[10] Malik, M.R.: Finite-Difference Solution of the Compressible Stability Eigenvalue Problem. NASA Contractor Report 3584, 1982.

11. Figure Captions

Figure 1: Parallel mean flow over a flat plate. The coordinate axes are labelled according to accepted nomenclature.

Figure 2: Mean profiles U_m (solid line) and T_m (dashed line) at Mach 0.5 (see table I) along the direction normal to the plate.

Figure 3: Mean profiles U_m (solid line) and T_m (dashed line) at Mach 0.5 (see table I) along the direction normal to the plate.

Figure 4: Mach 0.5 complex eigenfunctions of the linearized compressible Navier-Stokes equations at R_e=1100 along the direction normal to the plate: u_{2D} (4a), u_{3D} (4b), T_{2D} (4c) and T_{3D} (4d).

Figure 5: Mach 4.5 complex eigenfunctions of the linearized compressible Navier-Stokes equations at R_e=10000 along the direction normal to the plate: u_{2D} (5a), u_{3D} (5b), T_{2D} (5c) and T_{3D} (5d).

Figure 6: Comparison of temperature eigenfunction profiles at Mach 0.5 (6a) and Mach 4.5 (6b).

Figure 7: Growth curves of perturbed kinetic energy at Mach 0.5 (case I) for 1/2 period with 33 collocation nodes (x), 33 (+), 65 (*) and 129 (x) finite-difference nodes. The 129 finite-difference, 33 collocation and the theoretical curve are indistinguishable from each other.

Figure 8: Growth curves of perturbed kinetic energy at Mach 4.5 (case II) for 1 period with 129 finite-difference nodes (*), and 33 (x) and 65 (O) collocation nodes. The theoretical curve is indistinguishable from the 65 spectral node curve.

Figure 9: Evolution of the kinetic energy of selected Fourier modes. The energy is plotted on a logarithmic scale.

Figure 10: Spanwise vorticity in successive spanwise planes after 5.5 periods (M_∞=4.5,R_e=10000.0). The planes are located at x=0 (10a), L_x/4 (10b), and L_x/2 (10c) where L_x is the streamwise period.

Figure 10c is the peak plane. The planar cuts extend to z=2 in the normal direction.

Figure 11: Spanwise vorticity in successive streamwise planes after 5.5 TS periods (M_∞=4.5,R_e=11000.0). The planes are located at y=0 (11a), $L_y/4$ (11b), $L_y/2$ (11c), and $3L_y/4$ (11d) where L_y is the spanwise period. The planar cuts extend to z=2 in the normal direction.

Figure 12: Streamwise vorticity in successive streamwise planes after 5.5 TS periods (M_∞=4.5,R_e=10000.0). The planes are located at y=0 (12a), $L_y/4$ (12b), $L_y/2$ (12c), and $3L_y/4$ (12d) where L_y is the spanwise period. The planar cuts extend to z=2 in the normal direction.

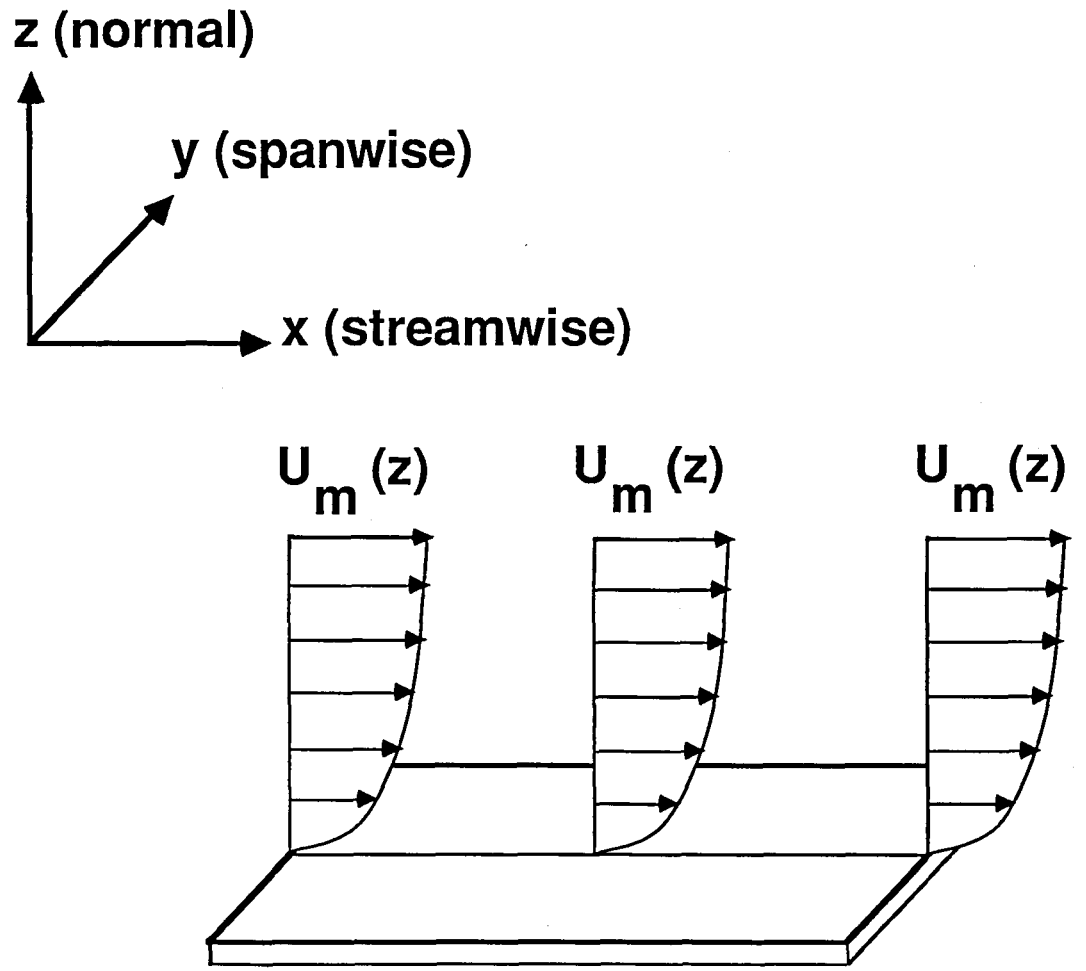

Figure 1

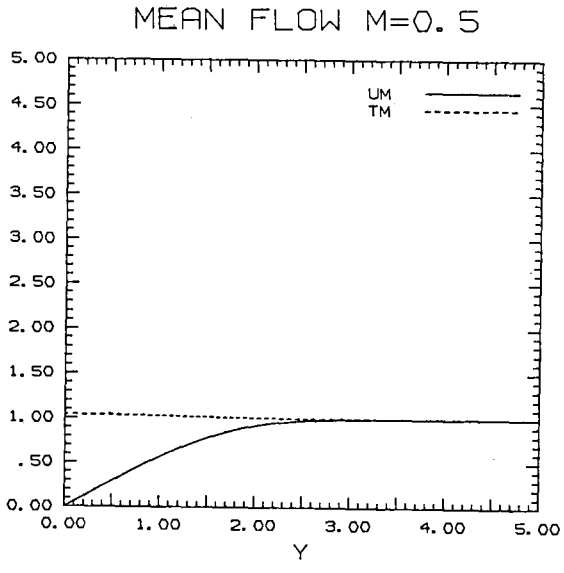

Figure 2

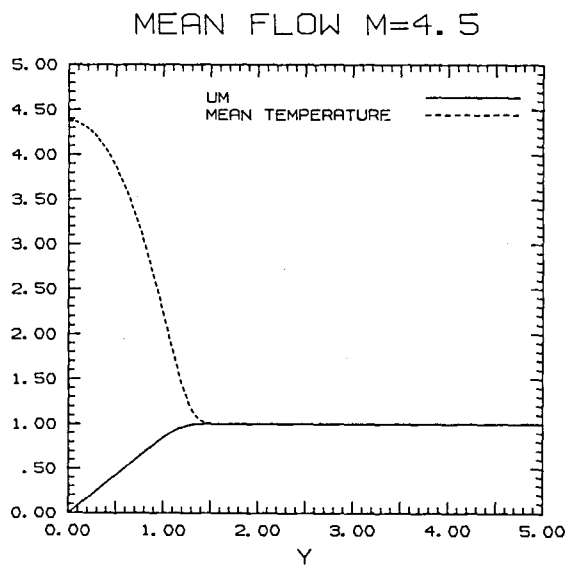

Figure 3

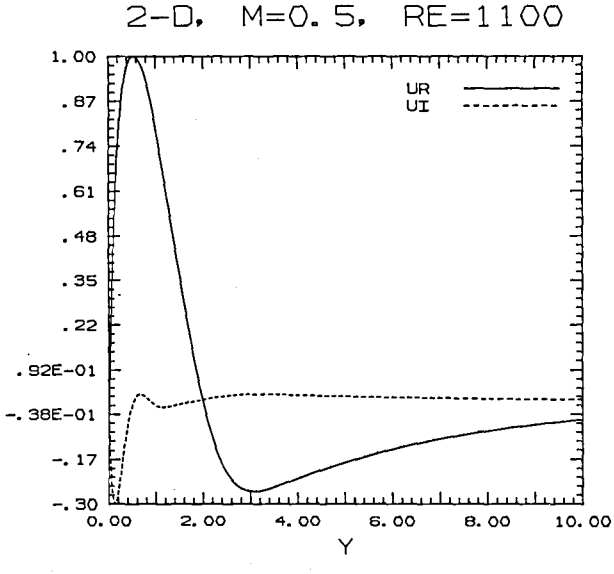

Figure 4a

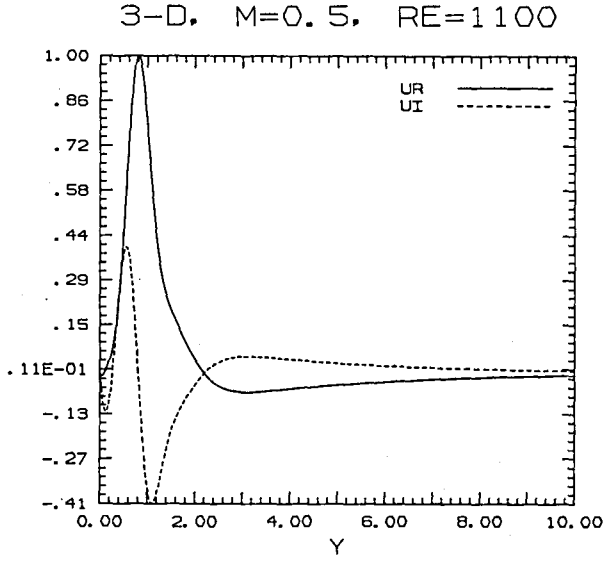

Figure 4b

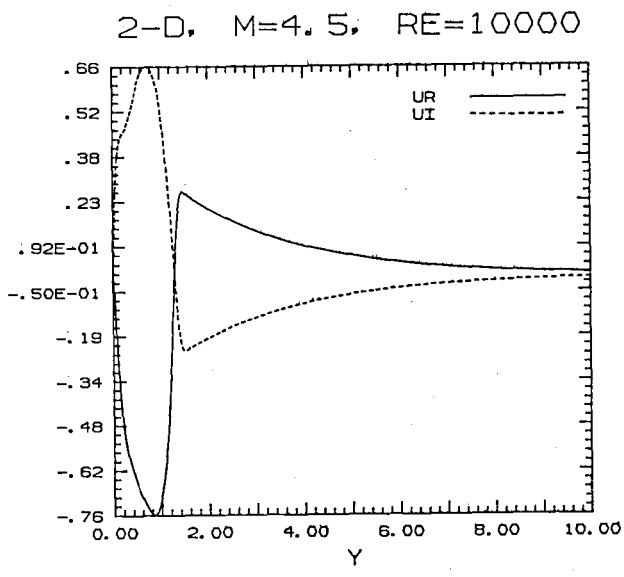

Figure 5a

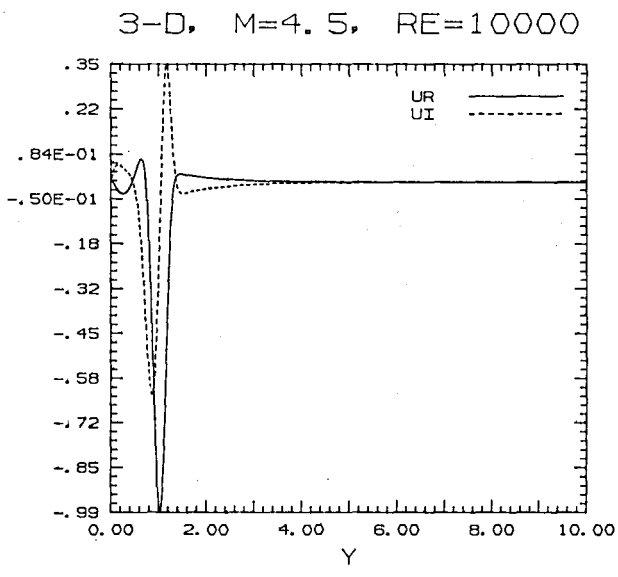

Figure 5b

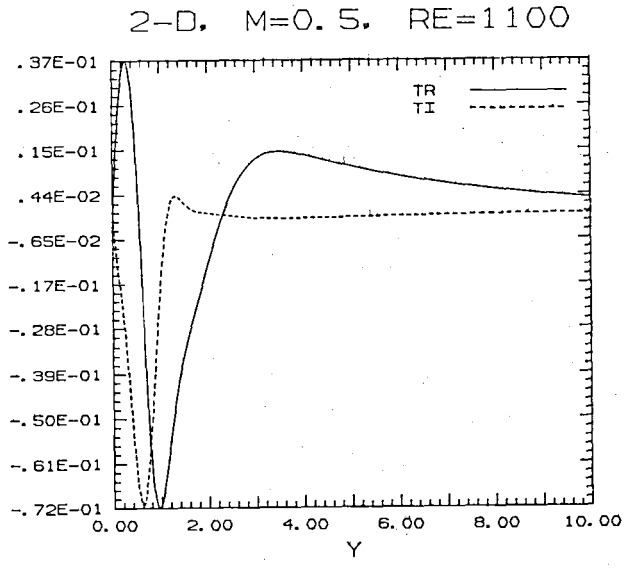

Figure 6a

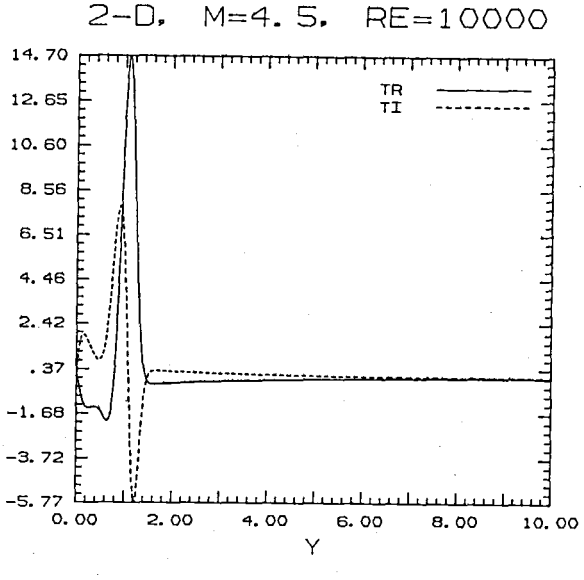

Figure 6b

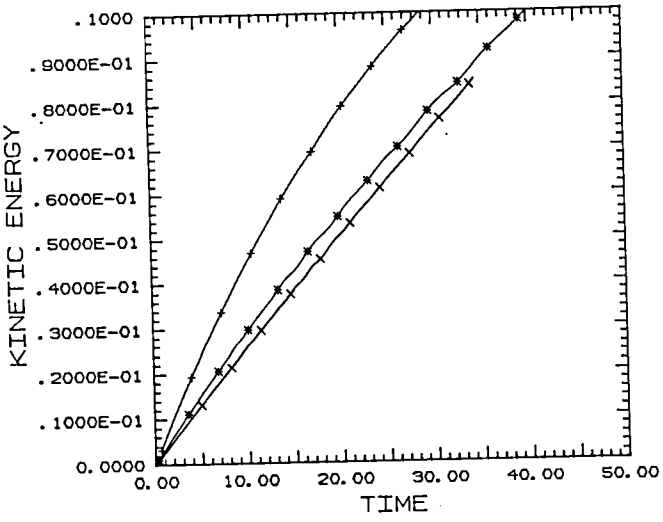

Figure 7

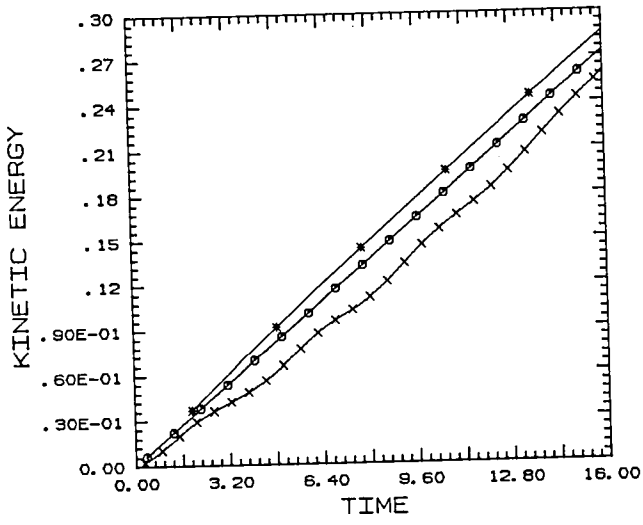

Figure 8

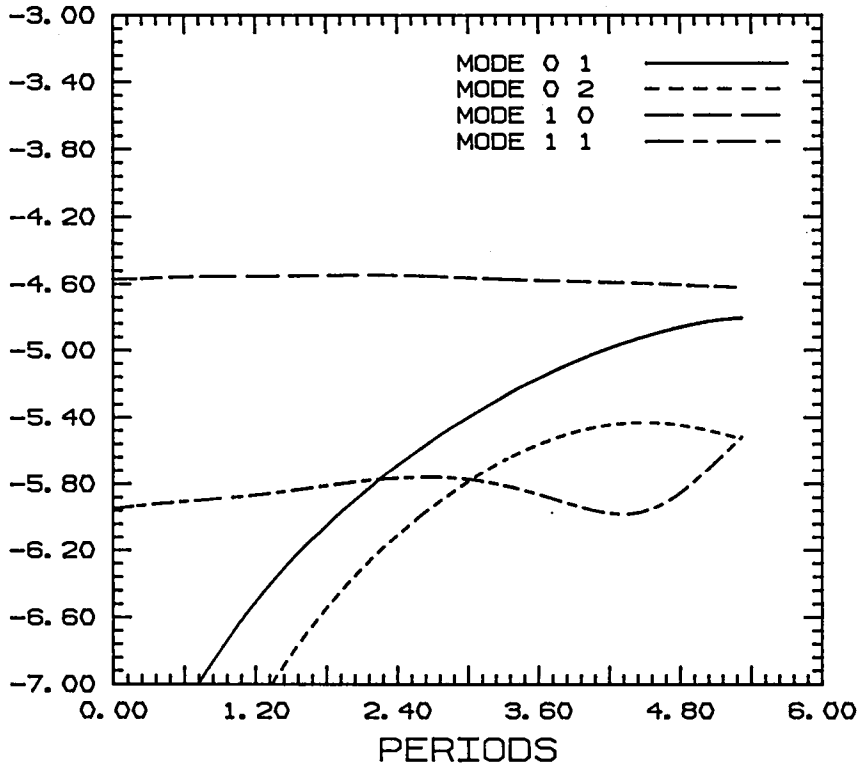

Figure 9

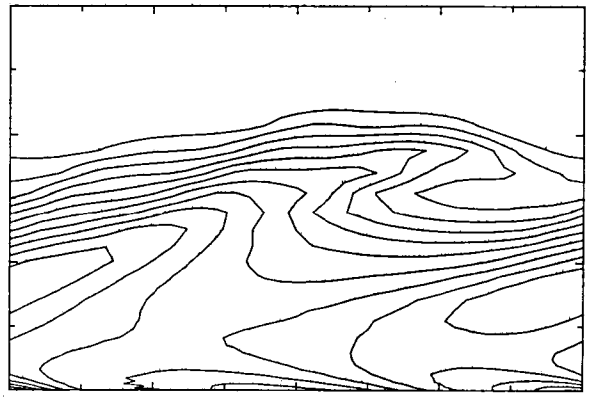

(a)

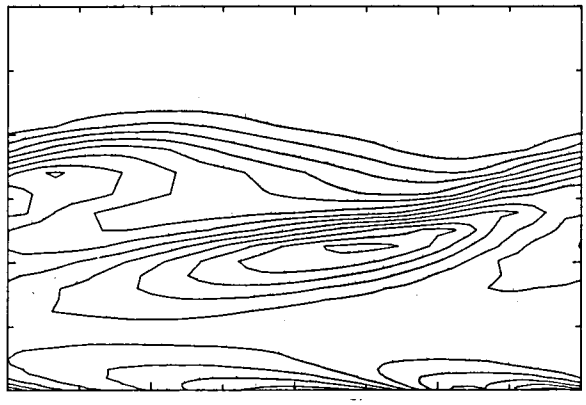

(b)

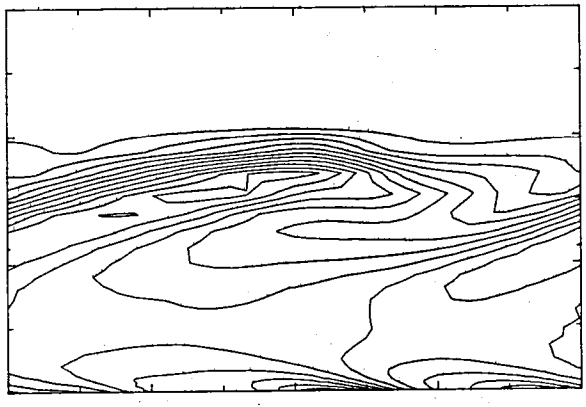

(c)

Figure 10

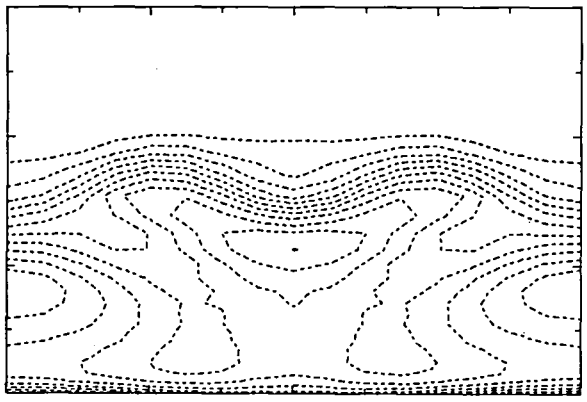

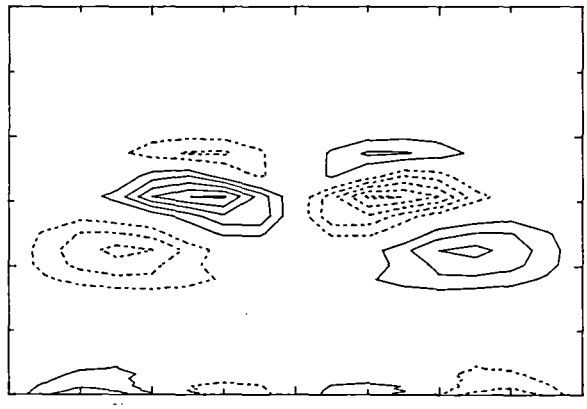

(a)

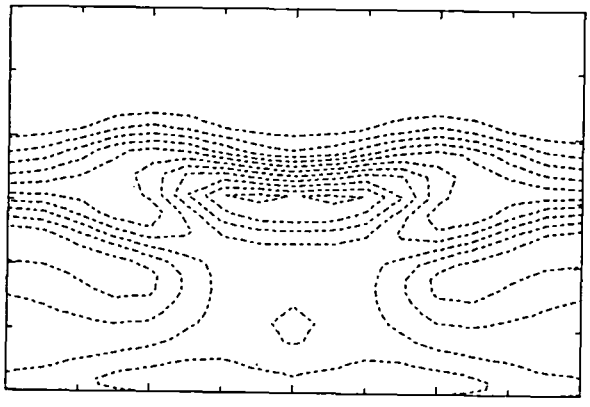

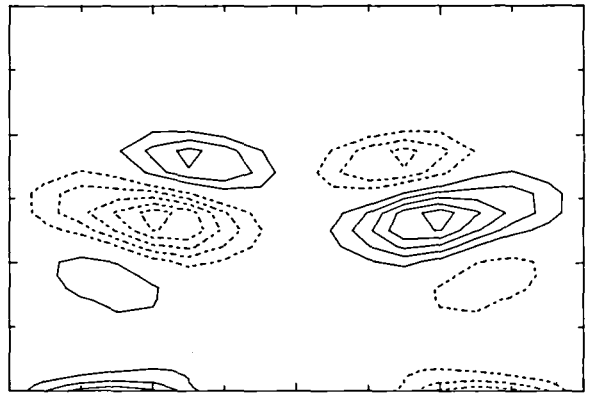

(b)

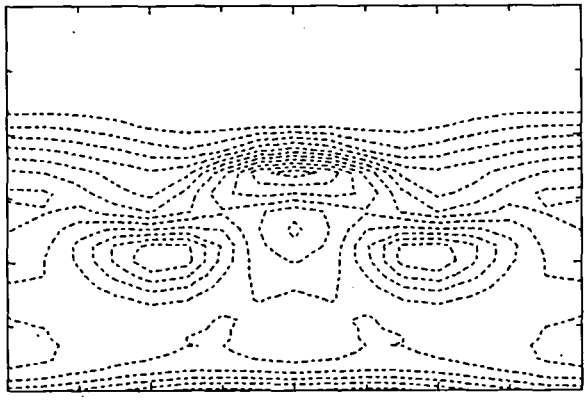

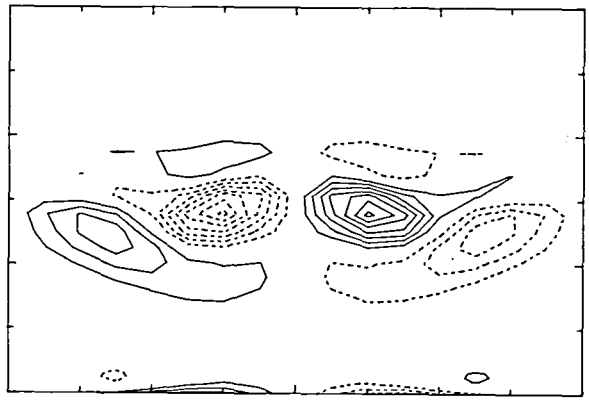

(c)

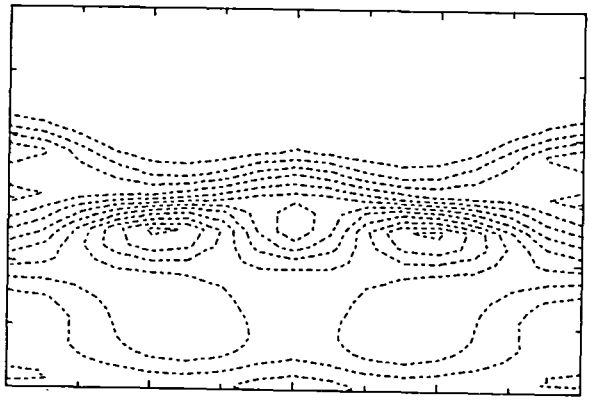

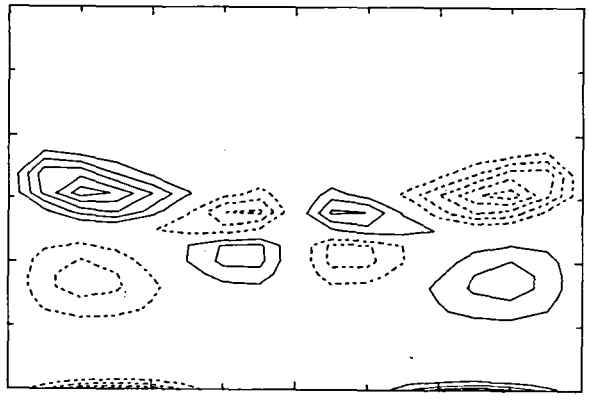

(d)

Figure 11

Figure 12

Standard Bibliographic Page

1. Report No. NASA CR-178111 ICASE Report No. 86-39	2. Government Accession No.	3. Recipient's Catalog No.
4. Title and Subtitle INCIPIENT TRANSITION PHENOMENA IN COMPRESSIBLE FLOWS OVER A FLAT PLATE		5. Report Date June 1986 6. Performing Organization Code
7. Author(s) Gordon Erlebacher and M. Yousuff Hussaini		8. Performing Organization Report No. 86-39
9. Performing Organization Name and Address Institute for Computer Applications in Science and Engineering Mail Stop 132C, NASA Langley Research Center Hampton, VA 23665-5225		10. Work Unit No. 11. Contract or Grant No. NAS1-17070, NAS1-18107
12. Sponsoring Agency Name and Address National Aeronautics and Space Administration Washington, D.C. 20546		13. Type of Report and Period Covered Contractor Report 14. Sponsoring Agency Code 505-31-83-01

15. Supplementary Notes

Langley Technical Monitor:
J. C. South

Final Report

Submitted to Proc. 10th Inter. Conf. on Num. Methods in Fluid Dynamics

16. Abstract

The full three-dimensional time-dependent compressible Navier-Stokes equations are solved by a Fourier-Chebychev method to study the stability of compressible flows over a flat plate. After the code is validated in the linear regime, it is applied to study the existence of the secondary instability mechanism in the supersonic regime.

17. Key Words (Suggested by Authors(s))	18. Distribution Statement
compressible Navier-Stokes equations, boundary layer, secondary instability	34 - Fluid Mechanics and Heat Transfer Unclassified - unlimited

19. Security Classif.(of this report)	20. Security Classif.(of this page)	21. No. of Pages	22. Price
Unclassified	Unclassified	21	A02

For sale by the National Technical Information Service, Springfield, Virginia 22161

NASA-Langley, 1986

End of Document